Recovery of gold by solvent extraction and direct electrodeposition using phosphonium-based ionic liquids

Masahiko MATSUMIYA[a*], Ryoma KINOSHITA[a], and Yuji SASAKI[b]

[a] Graduate School of Environment and Information Sciences, Yokohama National University, 79-2 Tokiwadai, Hodogaya-ku, Yokohama 240-8501, Japan

[b] Nuclear Science and Engineering Directorate, Japan Atomic Energy Agency, Tokai-mura, Naka-gun, Ibaraki, 319-1195, Japan

[*] Corresponding author
E-mail address: matsumiya-masahiko-dh@ynu.ac.jp
Tel : +81-45-339-3464

ABSTRACT

In this study, phosphonium-based ionic liquids (IL), i.e., triethyl-*n*-pentyl, triethyl-*n*-octyl, and triethyl-*n*-dodecyl phosphonium bis(trifluoromethyl-sulfonyl)amide, $[P_{222X}][NTf_2]$, (X=5, 8, and 12) were investigated for Au(III) extraction. The IL–Au complex was identified as $[P_{2225}][AuCl_4]$ using UV–Vis–NIR and Raman spectroscopic analyses. Slope analyses with the concentration dependence of $[P_{222X}^+]$ confirmed the anion-exchange mechanism of Au(III) extraction by $[P_{222X}^+]$ (X=5, 8, and 12). The enthalpy, entropy, and Gibbs free energy for Au(III) extraction were determined using thermodynamic analysis, indicating that lower temperatures had a positive effect on the Au(III) extraction.

Electrochemical analysis revealed that extracted Au(III) can be reduced in two steps: (i)Au(III) + $2e^-$ → Au(I), (ii) Au(I) + e^- → Au(0)]. The diffusion coefficients of the extracted Au(III) species in $[P_{222X}][NTf_2]$ (X=5, 8, and 12) were evaluated from 323 to 373 K using semi-integral and semi-differential analyses. Because of the viscosity of the IL medium, the diffusion coefficient of the extracted Au(III) increases with increasing alkyl chain length. The $4f_{7/2}$ spectrum based on X-ray photoelectron spectroscopy revealed that the Au electrodeposits obtained after 10 cycles of continuous extraction and electrodeposition were in the metallic state.

Keywords**:** Au(III), Electrodeposition, Ionic liquid, Solvent extraction

1. Introduction

Room-temperature ionic liquids (ILs) exhibit unique properties such as incombustibility, low vapor pressure, high ionic conductivity, and a wide electrochemical window [1,2]. Compared to general solvents, hydrophobic ILs are advantageous for operations conducted in an open system at variable temperatures, without the release of harmful vapors or hydrogen embrittlement [3,4]. In particular, phosphonium-based ILs with short alkyl chains have the advantages of low viscosity and a wider cathodic limit on the electrochemical window than imidazolium- and ammonium-based ILs.

Numerical processes have been developed for metal recovery from various effluents. Solvent extraction (SX) / stripping processes, followed by electrowinning of the metal from the loaded stripping solution, have been proposed as useful methods for the selective removal and recovery of noble metals. Silver recovery from acidic solution using SX, followed by the electrochemical stripping of the extracted Ag(I)-calixarene complex is one of the methods reported [5]. Furthermore, we could show that SX and electrodeposition (ED) can recover Ru [6], Ir [7], and Pt [8] metals from phosphonium-based ILs. This novel SX–ED process using an IL has several advantages, including the elimination of numerous complex processing steps, reduced secondary waste generation, reduced environmental risk, a significant volume reduction, and easy handling of the electrodeposits.

Au is the most important element, as well as a non-substitutable and indispensable strategic resource. In conventional hydrometallurgical processes, Au dissociates as Au(III) in acidic medium. Recently, studies have been conducted on Au(III) extraction using ILs as extractants or diluents. ILs such as piperidinium, pyrrolidinium, and pyridinium have been studied as extractants for noble metal extractions [9–13]. Thus, it is effective to extract trace amounts of Au(III) using these ILs. Furthermore, the polarity, hydrophobicity, and solvent miscibility of these ILs can be adjusted depending on their intended use. Therefore, the unique properties of ILs make them promising functional extraction media for SX. The uses of ILs as alternatives to organic solvents has been extensively studied in various fields. However, the extraction mechanism of Au(III) using phosphonium-based ILs and relevant thermodynamic studies are yet to be reported. In the present work, we focused on the mechanism of Au(III) extraction and related thermodynamic analyses using

phosphonium-based ILs: triethyl-*n*-pentyl, triethyl-*n*-octyl, and triethyl-*n*-dodecyl phosphonium bis(trifluoromethylsulfonyl)amide, [P_{222X}][NTf_2], (X=5, 8, and 12).

Furthermore, to analyze the electrodeposition behavior of Au metal from the extracted Au(III) complex in a phosphonium-based IL, the diffusion coefficients and activation energies for diffusion in [P_{2225}][NTf_2] were estimated from the semi-integral (SI) and semi-differential (SD) analyses of the voltammograms. In addition, we attempted to directly electrodeposit Au metal from the loaded IL bath, including the Au(III) complex. The reusability of the IL medium was also evaluated using the continuous SX–ED process for 10 cycles. Finally, the electrodeposited metal was characterized by X-ray photoelectron spectroscopy (XPS).

2. Experimental

2.1 Sample preparation

ILs triethyl-*n*-pentylphosphonium bis(trifluoromethyl-sulfonyl)amide ([P_{2225}][NTf_2]), trioctyl-*n*-pentylphosphonium bis(trifluoromethyl-sulfonyl)amide ([P_{2228}][NTf_2]), and tridodecyl-*n*-pentylphosphonium bis(trifluoromethyl-sulfonyl)amide ([P_{22212}][NTf_2]) were synthesized by the metathesis reaction of [P_{222X}]Br (X=5, 8, and 12) (Nippon Chemical Industrial Co., Ltd., >99.5%) and Li[NTf_2] (Kanto Chemical Co., Inc., 99.7%), as described in a previous work [14]. The absence of halogen ions in IL was confirmed using $AgNO_3$ after repeatedly washing the IL with distilled water. The obtained IL was dried under vacuum < −0.1 MPa at 393 K for > 48 h. The average yield of the IL was greater than 90%. The aqueous phases of the [$AuCl_4^-$], [$PtCl_6^{2-}$], [$PdCl_4^{2-}$], and [$IrCl_6^{2-}$] samples were prepared by dissolving an appropriate amount of anhydrous $AuCl_3 \cdot 4H_2O$ (2N, Kishida Chemical Co., Ltd.), H_2Cl_6Pt (Fujifilm Wako Pure Chemical Co. Ltd., >97.0%), $PdCl_2$ (Fujifilm Wako Pure Chemical Co. Ltd., >98.0%), and anhydrous $IrCl_4$ (2N, Koujundo Chemical Laboratory Co. Ltd.) in hydrochloric acid, respectively.

2.2 Solvent extraction

The ILs triethyl-*n*-pentyl, triethyl-*n*-octyl, and triethyl-*n*-dodecyl phosphonium

bis(trifluoromethyl-sulfonyl)amide, $[P_{222X}][NTf_2]$ (X=5, 8, and 12) were used as the extractants for both the precious metals and diluents. SX was performed using IL, and the extraction studies were conducted with a 1:1 IL to aqueous phase volume ratio. A sealed system was used for the extraction procedure. The operating temperature was changed from 298 K to 368 K. The extraction process was stirred at 350 rpm for 12 h. To determine the stoichiometry of the extracted metal complex, the extraction behavior of Au(III) as a function of variation of the $[P_{222X}][NTf_2]$ (X=5, 8, and 12) was studied. The concentration of $[P_{222X}][NTf_2]$ (X=5, 8 and 12) was varied from 1.0×10^{-4} to 1.0×10^{-1} mol dm^{-3} for dichloromethane (Fujifilm Wako Pure Chemical Co. Ltd., >98.0%) while fixing the aqueous phase. The concentration of the extracted Au(III) complex was determined from the extraction percentage after calculating the extraction equilibrium constants of $[AuCl_4^-]$ and $[P_{2225}][NTf_2]$. The concentrations of the ILs (100% pure) were calculated from the molar number and volume. After equilibration, the concentration of the metallic species in the aqueous phase was measured using inductively coupled plasma atomic emission spectroscopy (ICP-–AES, ICPE–9000, Shimadzu Co.). The distribution ratio (D) and extraction efficiency (E) were calculated based on ICP–AES quantitative data using Eq. (1).

$$D=\frac{[M]_{aq}^{ini}-[M]_{aq}^{fin}}{[M]_{aq}^{fin}},\quad E(\%)=\frac{100D}{D+V_{aq}/V_{IL}} \tag{1}$$

where [M] and V represent the concentration of each metal ion and volume, respectively. The subscripts “aq” and “IL” represent aqueous and IL phases, respectively. The superscripts “ini” and “fin” represent the initial and final concentrations, respectively.

2.3 UV-Vis-NIR and Raman spectroscopy

The following samples of $[AuCl_4^-]$ were prepared in the aqueous phase: 4.9, 9.8, 24.6, 48.2 and 99.2 mg L^{-1} for ultraviolet–visible–near infrared (UV–Vis–NIR) spectroscopy. 2.5 mmol dm^{-3} of $[AuCl_4][P_{2225}]$ was prepared in the IL phase using the SX procedure. After the SX procedure,

$[AuCl_4][P_{2225}]$ sample was vacuum dried at 393 K for 48 h. Spectrophotometric measurements were conducted to determine the complexation of Au(III) in aqueous and IL phases. A UV–Vis–NIR spectrometer (Lamda720, Perkin Elmer Co., Ltd) with a quartz cell of 1.0 cm optical path length was used. Deuterium and halogen lamps were used as light sources in the UV and Vis–NIR regions, respectively. The obtained UV–Vis–NIR spectrum was deconvoluted with Gaussian function using the Origin 9.1 software.

A 532 nm laser was used to record Raman spectra (inVia reflex, RENISHAW) in the temperature range of 298–368 K. 1800 mm^{-1} was the appropriate grating for recording the Raman spectra. This condition was adopted to prevent fluorescence of the related ions, and was selected based on the findings of our recent studies [15]. To increase the signal-to-noise ratio, the Raman spectra were measured by averaging 512 individual measurements. The overlapping Raman bands were deconvoluted into individual components using the pseudo-Voigt function.

2.4 Electrochemical measurement

The sample was vacuum dried at 393 K for 48 h after the SX procedure, before electrochemical measurements. Cyclic voltammetry (CV) was performed using a three-electrode system inside a cylindrical cell. A Pt disk electrode with a diameter of 1.6 mm was used as the working electrode. The electrode surface was polished with alumina paste (d = 0.05 μm) and diamond paste (d = 1 μm) before measurements. Pt wires with diameters of 0.5 mm were used as counter and quasi-reference electrodes (QRE) because the potential obtained using a Pt QRE was stable and exhibited good reproducibility at elevated temperatures. The potential was compensated for the IL standard using a ferrocene (Fc)/ferrocenium (Fc^+) redox couple. CV measurements were carried out at different temperatures (323, 333, 343, 353, 363, and 373 ± 1.0 K) using an electrochemical analyzer (ALS-760E, BAS Inc.). The extracted Au(III) species dissolved in $[P_{222X}][NTf_2]$ (X=5, 8, and 12) was vacuum dried at 373 K for 48 h and used as the electrolyte for CV analysis. Using Karl–Fischer moisture titrator (MKC-610-NT/ADP-611, Kyoto Electronics Manufacturing Co., Ltd.), the water content of the IL, including the extracted Au(III) complex, was found to be less than 50 ppm.

Electrochemical measurements were conducted under an Ar atmosphere in a glovebox (DBO-1KP-YUM01, MIWA Inc.).

2.5 Continuous solvent extraction (SX) and electrodeposition (ED)

To evaluate the reusability of $[P_{2225}][NTf_2]$ medium, a recycling run consisting of 10 cycles of SX and ED was performed. For SX, 1.0×10^3 mg L^{-1} Au(III) was used as the aqueous phase because a continuous SX–ED process was needed to enrich the metal concentration in the IL phase. The volume ratio of the aqueous and IL phases was maintained at 3.0. After the SX process, ED of Au metal from the extracted Au(III) complex in the $[P_{2225}][NTf_2]$ medium was carried out using a three-electrode system inside a cylindrical cell at 298 K under an Ar atmosphere. A Pt wire and Cu substrate were employed as the anode and cathode, respectively. The anode was surrounded by a soda lime tube with a Vycor glass filter at the bottom to prevent the diffusion of the decomposition products from the anode into the electrolyte. The QRE composed of a Pt wire with a diameter of 0.5 mm. For the potentiostatic ED, the overpotential applied to the cathode was -1.25 V versus Fc/Fc^+ relative to the extracted media. After ED, all electrodes from the electrolytic bath were replaced, and the electrolytic bath was reused for the next stages of SX. In the next SX process, a new aqueous phase containing 1.0×10^3 mg L^{-1} Au(III) was introduced into the IL phase. After the second SX, ED was conducted at the same overpotential. Thus, the procedure for SX and ED was repeated for 10 cycles. After the continuous SX–ED cycle, the metal concentration in the IL phase for each cycle was analyzed using ICP–AES. Current efficiency was calculated based on the increase in weight of the cathode after each ED. The metallic state of Au in the electrodeposits was evaluated by XPS (Quantera SXM, ULVAC-PHI, Inc.) to investigate the chemical bonding state and ratio of each element. The electrodeposited samples were transported to the XPS equipment without exposure to the atmosphere using a transfer vessel to prevent the oxidation of the deposited surface. The detection angle from the sample surface was set to 45°. The sample on the substrate was analyzed by etching using an Ar ion beam.

3. Results and Discussion

3.1 Complexation state of Au(III)

Understanding the complexation state of Au(III) in the aqueous phase is crucial. In the aqueous phase, the six Au(III) complexes, i.e., [$AuCl_4^-$], [$AuCl_3(H_2O)$], [$AuCl_3(OH)^-$], [$AuCl_2(OH)_2^-$], [$AuCl(OH)_3^-$], and [$Au(OH)_4^-$], are tetragonal species. The equilibrium constants, K_1 to K_6, for the six Au(III) complexes have been previously reported [16] and listed in **Table 1**. The distribution of these complexes calculated from the corresponding equilibrium constants are shown in **Fig. 1**, and the primary Au(III) complex at pH<1.0 was found to be [$AuCl_4^-$].

The UV–Vis–NIR spectra of the aqueous phase, including Au(III) at different concentrations is shown in **Fig. 2**. There are two peaks at 227 and 314 nm in the spectrum, which corresponds to the *d-d* transitions [$^1A_{1g}\rightarrow{}^1E_u(\sigma)$] and [$^1A_{1g}\rightarrow{}^1A_{2u}+{}^1E_u(\pi)$] [17], as listed in **Table 2**. The absorbance was proportional to the concentration of the Au(III) complex and satisfied Lambert–Beer's law, as shown in the inset of Fig. 2. The molar extinction coefficients were found to be in general agreement with the reference data [17]. This result indicates that in the aqueous phase, the dominant species in the HCl medium was [$AuCl_4^-$], which is consistent with the distribution result shown in Fig. 1. Thus, the UV–Vis–NIR analysis is a good indicator of the complexation state in the aqueous phase. Furthermore, the UV–Vis–NIR spectrum of the bright yellow colored IL–Au complex is shown in **Fig. 3**. The absorption of the IL–Au complex at 320 nm corresponds to *d-d* transition [$^1A_{1g}\rightarrow{}^1A_{2u}+{}^1E_u(\pi)$] and belongs to [$AuCl_4^-$]. This result indicates that the coordination environment of Au(III) did not change during the formation of the IL–Au complex.

The Raman spectrum of the extracted Au(III) in [P_{2225}][NTf_2] system is shown in **Fig. 4**. It is well known that the intense band at around 740 cm^{-1} in the Raman spectrum of the [NTf_2^-] anion in the IL can be assigned to the CF_3 bending vibration $\delta_s(CF_3)$ coupled with the S–N stretching vibration ν_s(SNS) [18]. This intense band was attributed to the free [NTf_2^-] anion, which did not coordinate with any metal cations. In the case of solvation with a metal cation [19], this intense band shifted to around 750 cm^{-1}. For the extracted Au(III) sample, the intensity remained almost constant with increasing operating temperature. However, no solvation [NTf_2^-] peak was observed at 750 cm^{-1}

for the extracted Au(III) sample. Consequently, the extracted Au(III) from $[P_{2225}][AuCl_4]$ complex, and the $[NTf_2^-]$ anion would not be solvated around the first coordination sphere at the center of the Au^{3+} cation. This result is consistent with the UV–Vis–NIR analysis.

3.2 Extraction behavior of Au(III)

It is important to understand the stoichiometry of the extracted metal complexes. The extraction behavior of Au(III) with a change in the $[P_{222X}][NTf_2]_{IL}$ (X=5, 8, and 12) concentration from 1.0×10^{-4} to 1.0×10^{-1} mol dm^{-3} is shown in **Fig. 5**. The extraction results indicate that Au(III) can be easily extracted by the anion-exchange reaction in the $[P_{222X}][NTf_2]_{IL}$ (X=5, 8, and 12). The slope range 0.96–1.01 on the plot of log *D* vs. $\log[P_{222X}][NTf_2]_{IL}$ (X=5, 8, and 12) indicates the association of one mole of IL with one mole of $[AuCl_4^-]$ during extraction. Consequently, $[P_{222X}][NTf_2]$ (X=5, 8, and 12) is an anion-exchange extractant for the extraction of Au(III) in the form of anions from chloride media.

Thus, this type of phosphonium-based IL proceeds via an anion-exchange reaction with Au(III), and the extraction mechanism for Au(III) with the $[P_{222X}][NTf_2]_{IL}$ (X=5, 8, and 12) can be expressed as follows:

$$[AuCl_4^-]_{aq} + [P_{222X}][NTf_2]_{IL} \rightleftarrows [P_{222X}][AuCl_4]_{IL} + [NTf_2^-]_{aq} \text{ (X=5, 8 and 12)} \qquad (2)$$

The extraction equilibrium constant (K_{ex}) and the distribution ratio (*D*) are expressed as follows.

$$K_{ex}=\frac{[P_{222X}][AuCl_4]_{IL}[NTf_2^-]_{aq}}{[AuCl_4^-]_{aq}[P_{222X}][NTf_2]_{IL}},\ D=\frac{[P_{222X}][AuCl_4]_{IL}}{[AuCl_4^-]_{aq}} \text{ (X=5, 8 and 12)} \qquad (3)$$

The following relationship is obtained from Eq. (3).

$$K_{ex}=\frac{D[NTf_2^-]_{aq}}{[P_{222X}][NTf_2]_{IL}} \quad (X=5, 8 \text{ and } 12) \tag{4}$$

The logarithm of D is expressed according to the relation in Eq. (4), as follows:

$$\log D = \log K_{ex} - \log[NTf_2^-]_{aq} + \log[P_{222X}][NTf_2]_{IL} = \log K_{ex}' + \log[P_{222X}][NTf_2]_{IL} \quad (X=5, 8 \text{ and } 12) \tag{5}$$

where $\log K_{ex}'$ is the apparent equilibrium constant evaluated from the intercept of $\log[P_{222X}][NTf_2]_{IL}$ (X=5, 8 and 12) versus $\log D$, as shown in Fig. 4. The calculated $\log K_{ex}'$ for $[P_{222X}][NTf_2]_{IL}$ (X=5, 8 and 12) were 2.332, 2.558 and 2.948, respectively. Although the viscosity of $[P_{222X}][NTf_2]_{IL}$ (X=5, 8 and 12) increased with the alkyl side chain length, the value of $\log K_{ex}'$ of $[P_{22212}][NTf_2]_{IL}$ became higher than that of $[P_{2225}][NTf_2]_{IL}$. The result indicates that the bulk properties did not influence the extraction performance of Au(III).

To evaluate the thermodynamic parameters on the Au(III) extraction, the equilibrium constant ($\log K_{ex}$') was determined from the temperature dependence:

$$\Delta G = -RT\ln K_{ex}' = \Delta H - T\Delta S \tag{6}$$

The plot of the natural logarithm of K_{ex}' versus the inverse of the absolute temperature (T^{-1}) yields a slope proportional to the enthalpy (ΔH).

$$\ln K_{ex}' = -\frac{\Delta H}{RT} + \frac{\Delta S}{R} \tag{7}$$

By plotting T^{-1} versus $\ln K_{ex}'$, a line with a slope range 1.129-1.421 was obtained, which is shown in **Fig. 6**. Thus, the result indicated that the extraction reaction of Au(III) using the $[P_{222X}][NTf_2]_{IL}$ (X=5, 8 and 12) was exothermic. The related thermodynamic properties are listed in **Table 3**. The negative value of $T\Delta S$ indicates that microscopic randomness is preferred in the $[P_{2225}][NTf_2]_{IL}$

extraction system over $[P_{22212}][NTf_2]_{IL}$. The total negative alternation in Gibbs energy for the extraction reaction would thus be relatively influenced by the $T\Delta S$ value on the number of carbon atoms in the alkyl side length, even if the efficiency of ΔH is significantly influenced by the total negative alternations in Gibbs energy. Thus, the thermodynamic properties of Au(III) in the $[P_{222X}][NTf_2]_{IL}$ (X=5, 8, and 12) system are similar to those in the $[C_{16mim}]Cl$ system [20]. The separation factors for the related platinum group metals are tabulated in **Table 4**. $[P_{2225}][NTf_2]_{IL}$ and $[P_{2228}][NTf_2]_{IL}$ were found to be effective for the separation of Au/Pt, and $[P_{22212}][NTf_2]_{IL}$ was found to be effective for the separation of Pt/Pd.

3.3 Electrochemical behavior of extracted Au(III) complex

The voltammetric analysis of Au(III) and $[P_{2225}][AuCl_4]$ in $[P_{2225}][NTf_2]$ was performed at various sweep rates, as shown in **Fig. 7**. Different potential scans were checked prior to peak B; however, only oxidation peak A' was observed. Two reduction peaks (A and B) around -0.464 V and -1.189 V and two oxidation peaks (A' and B') around 0.285 V and -0.328 V in the voltammogram were observed. Reduction peaks A and B at approximately -0.464 V and -1.189 V, respectively, would result from the following two-step reactions:

$$Au(III) + 2e^- \rightarrow Au(I) \text{ (peak A)} \quad (8)$$

$$Au(I) + e^- \rightarrow Au(0) \text{ (peak B)} \quad (9)$$

Assuming that each peak in the voltammogram is based on cathodic reactions (8) and (9), we confirmed that the cathodic peak plot of the current density (j_p) versus the square root of the potential sweep rate ($v^{1/2}$) demonstrated a strong linear relationship. This result indicates that both reduction reactions, (8) and (9), were controlled by diffusion using a Pt electrode, i.e., mass transport under semi-infinite linear diffusion conditions. In addition, the slope of the j_p versus $v^{1/2}$ plot is different for the two reactions, which indicates that there is a difference in the diffusion coefficient of the extracted complex, Au(III). Therefore, the diffusion coefficients of the extracted Au(III) in

$[P_{2225}][NTf_2]$ were estimated from an SI analysis of the voltammogram. Both mass and charge transfer processes are crucial while analyzing the rates of electrode reaction.. Particularly, mass transfer by diffusion is a principal factor in determining the aspects of the electrode reaction in IL solvents. Therefore, it is necessary to evaluate the diffusion coefficient of the extracted Au(III) in $[P_{2225}][NTf_2]$ when considering the ED of Au metal. Analyzing the limiting current in the SI analysis enabled us to evaluate the diffusion coefficient of the extracted Au(III) accurately in an irreversible process. The SI curves obtained from the voltammograms of the extracted Au(III) in $[P_{2225}][NTf_2]$ at 323 K are shown in **Fig. 8**. The SI analysis revealed two plateaus, which correspond to the reduction peaks A and B. Conventionally, the SI limitation current, m*, was estimated by subtracting the background current. The diffusion coefficient was calculated from the value of m^*, according to the following equation [21,22]:

$$m^*=nFAD^{1/2}C^* \tag{10}$$

where n is the number of electrons involved in the charge transfer reaction, F is the Faraday constant, A is the electrode surface area, D is the diffusion coefficient of the electrochemical oxidant species, and C^* is the bulk concentration of the electroactive species. The diffusion coefficient of the extracted Au(III) complex can be calculated from the values of m_A^* and C_A^* because the bulk concentration of the extracted Au(III) was analyzed using ICP–AES. The diffusion coefficient of Au(I) cannot be estimated from the value of m_B^* because the bulk concentration of the extracted Au(I) cannot be determined under this condition. As a result, the diffusion coefficients of the extracted Au(III) in $[P_{222X}][NTf_2]$ (X=5, 8, and 12) at 323 K were evaluated as 3.55×10^{-11}, 2.33×10^{-11} and 1.16×10^{-11} m^2 s^{-1}, respectively. The diffusion coefficient of the extracted Au(III) in $[P_{2225}][NTf_2]$ was greater than that in $[P_{2228}][NTf_2]$ and $[P_{22212}][NTf_2]$ over the entire range of operating temperatures. This result could be attributed to the fact that the extracted $[P_{222X}][AuCl_4]$ (X=8 or 12) is bulkier than the extracted $[P_{2225}][AuCl_4]$. The viscosity of $[P_{2225}][NTf_2]$ (88 mPa s) is the lowest compared with those of $[P_{2228}][NTf_2]$ (129 mPa s) and $[P_{22212}][NTf_2]$ (180 mPa s) because

the diffusion coefficient is mainly influenced by the viscosity of the medium according to Stokes–Einstein's law.

Furthermore, the standard rate constant k_s can be obtained using the following equation [21,22]:

$$E=E_s+\frac{RT}{\alpha nF}\ln\left(\frac{k_s}{D^{1/2}}\right)+\frac{RT}{\alpha nF}\ln\left\{\frac{m^*-m(t)}{i(t)}\right\} \quad (11)$$

where E is the electrode potential, E_s is the standard reversible potential of the reaction, R is the gas constant, T is the thermodynamic temperature, α is the transfer coefficient, m is the current SI, and i is the Faradaic current. The value of αn was calculated from the slope of the E versus $\log[m^*-m(t)]/i(t)$ plots, and k_s was determined from the intercept of the plots. Matsuda and Ayabe reported that in the case of an irreversible reaction, the following equation is satisfied [23]:

$$\frac{k_s}{(DvnF/RT)^{1/2}}<10^{-2(1+\alpha)} \quad (12)$$

where, v is the potential scan rate. Therefore, the following relationship was obtained by deformation with the substitution of the clear value in Eq. (11):

$$k_s < 1.60\times10^{-8}\ \text{m s}^{-1} \quad (13)$$

The k_s value calculated from the intercept of the E versus $\log[m^*-m(t)]/i(t)$ plots was 1.01×10^{-8} m s^{-1}. Accordingly, the reduction reaction of the extracted Au(III) in $[P_{2225}][NTf_2]$ at 323 K was deduced to be an irreversible process.

SD analysis was applied to the cyclic voltammogram of the extracted Au(III) in $[P_{2225}][NTf_2]$, as shown in **Fig. 9**. The SD peak width at half its height, W_p, and the current SD peak current density, e_p, at the peak of the SD polarogram were determined by the SD analysis of the voltammogram. The diffusion coefficient of the extracted Au(III) was calculated using the following equations [24], which were established in the case of an irreversible reaction:

$$W_{\mathrm{p}}=\frac{2.94RT}{\alpha nF},\ e_{\mathrm{p}}=\frac{\alpha n^2F^2AvC^*D^{1/2}}{3.367RT} \quad (14)$$

The diffusion coefficient of the extracted Au(III) in $[P_{2225}][NTf_2]$ at 323 K determined based on the SD analysis was found to be 3.24×10^{-11} m^2 s^{-1}, which is close to the value derived from the SI analysis. This congruence suggests the high reliability of the calculated diffusion coefficient of the extracted Au(III) in $[P_{2225}][NTf_2]$ derived from the SI and SD analyses.

The activation energy for diffusion using the diffusion coefficient values was then evaluated from the temperature dependences. The transfer of metallic cations in an electrolytic solution is generally affected by their electrostatic interactions with the ions constituting the metal complexes. Therefore, the diffusion of metallic cations in ILs requires a higher activation energy than the dissociation energy associated with the anions surrounding the metal complexes. The temperature dependence is conventionally expressed by the Vogel–Tammann–Fulcher (VTF) equation [25–27]:

$$D=D_0\exp[B_D/T-T_{0,D}] \quad (15)$$

where D_0 is a pre-exponential constant proportional to the diffusion coefficient, B_D is the pseudo-activation energy for diffusion, T is the absolute temperature, and $T_{0,D}$ is the ideal glass transition temperature. D_0, B_D, and $T_{0,D}$ are empirical material dependence parameters. The VTF plot is shown in **Fig. 10** with the best-fitting VTF lines. The fitting VTF parameters for extracted Au(III) in $[P_{222X}][NTf_2]$ (X=5, 8, and 12) are listed in **Table 5**. The B_D value of the extracted Au(III) negatively increased and the $T_{0,D}$ value monotonically decreased with increasing alkyl chain length of the cation in the IL medium. The B_D parameter generally corresponds to the activation energy of the diffusion behavior. The viscosity of the IL medium increased with increasing alkyl chain length of IL medium, as listed in Table 5. The decrease in the diffusion coefficient of the extracted Au(III) with increasing alkyl chain length influences the activation energy of diffusion due to the viscosity of the IL medium. The dependence of the B_D parameter on the alkyl chain length was reported for

imidazolium-based ILs [28] and is consistent with our results. Previously, we evaluated the charges of cations for $[P_{222X}][NTf_2]$ (X=5,8,12) from *ab initio* MO calculations. The calculated cationic charges of $[P_{2225}]$, $[P_{2228}]$ and $[P_{22212}]$ were 0.797, 0.798, and 0.798, respectively [29]. This result indicates that a higher diffusion coefficient of Au(III) in $[P_{2225}][NTf_2]$ would be effective for the recovery of Au during the ED process, although the electrostatic interaction of Au(III) with the anion might be similar.

3.5 Consecutive solvent extraction (SX) and electrodeposition (ED)

Continuous SX–ED processes were performed for 10 cycles to investigate the reusability of the $[P_{2225}][NTf_2]$ medium. The results of the SX–ED processes are listed in **Table 6**. A high extraction percentage (87.0–99.4%) was maintained for the 10 cycles of SX. A high extraction performance implies that no decomposition reaction occurred in the IL bath during each ED process, and the IL bath can be reused for the SX process after each ED process. The cathodic current efficiency was then maintained at a relatively high percentage (80.3−89.3%) for the first five cycles of the ED process. However, Cl^- might have liberated from $[P_{2225}][Cl]$ with P_{2225}^+, while $[AuCl_4]^-$ gradually reduced to Au metal during electrodeposition. A small amount of $[P_{2225}][Cl]$ might have dissolved in the aqueous phase during the following cycle of SX, resulting in the loss of IL. The reduction reaction of the extracted Au(III) proceeded smoothly in the IL bath. The recovery yield (82.7–88.3%) of Au metal was good for the first six cycles, thus it can be concluded that SX–ED is an effective process. EDX mapping showed a very small amount of oxygen deposited on the electrodeposited Au metal surface. This confirmed that the majority of the electrodeposited Au was composed of the metallic state. The amounts of carbon and oxygen detected by EDX were obtained from the Cu substrate. In summary, these results demonstrate that the top surface of electrodeposited Au contains a large amount of the metallic state and a smaller amount of the oxidized state. XPS was used to perform an in-depth analysis of the electrodeposited Au using Al-Kα radiation. The Au-4$f_{7/2}$ spectrum for the middle layer (< 0.5 μm) of the electrodeposits is shown in **Fig. 11**. The XPS analysis of the inner part of the electrodeposits was performed using Ar sputtering. The sputtering

rate was 27.2 nm min^{-1}. Theoretically, the Au-4$f_{7/2}$ peaks for Au metal and oxides should be positioned at 84.0 and 85.5 eV, respectively [30]. As seen in Fig. 11, the Au-4$f_{7/2}$ peaks of the electrodeposits have a binding energy in the range 84.0–84.1 eV, which hardly shifted before and after the Ar etching. The Au-4$f_{7/2}$ spectra of the top surface and the middle layer showed a relatively good agreement with the theoretical value based on Faraday's law. In this study, a series of analyses on Au electrodeposits led to the conclusion that most of the metallic Au can be recovered from a phosphonium-based IL by ED. The experimental results conclude that Au metal can be obtained from the direct ED of the extracted Au(III) in $[P_{2225}][NTf_2]$ medium.

4. Conclusion

In this study, phosphonium-based ILs i.e., triethyl-*n*-pentyl, triethyl-*n*-octyl, triethyl-*n*-dodecyl, and bis(trifluoromethylaulfonyl)amide, $[P_{222X}][NTf_2]$, (X=5, 8, and 12) without any added extractants were investigated for solvent extraction (SX) of precious metals. According to UV–Vis–NIR and Raman spectroscopic analyses of the extracted Au(III) complex, the $[P_{2225}][AuCl_4]$ complex forms in the IL medium, and the $[NTf_2^-]$ anion is not solvated around the first coordination sphere at the center of Au^{3+} cation.

The phosphonium-based ILs exhibited high Au (III) extractability. The extraction mechanism is considered to be an anion-exchange reaction: $[AuCl_4^-]_{aq} + [P_{222X}][NTf_2]_{IL} \rightleftarrows [P_{222X}][AuCl_4]_{IL} + [NTf_2^-]_{aq}$, (X=5, 8, and 12). Moreover, thermodynamic characteristics were evaluated at different operating temperatures. The Van't Hoff plot yielded a slope proportional to the enthalpy (ΔH), and the extraction reaction of Au(III) using $[P_{222X}][NTf_2]_{IL}$ (X=5, 8, and 12) was exothermic. The thermodynamic properties of Au(III) in the $[P_{222X}][NTf_2]_{IL}$ (X=5, 8, and 12) system were similar to those in the $[C_{16mim}]Cl$ system.

The diffusion behavior of the extracted Au(III) complex in the IL was investigated by CV. The results obtained from the voltammogram indicate that reduction of the extracted Au(III) complex proceeds in two steps: (i)Au(III) + $2e^-$ → Au(I), (ii) Au(I) + e^- → Au(0)]. SI and SD analyses were applied to calculate the diffusion coefficient of the extracted Au(III) complex in the IL. The obtained

diffusion coefficient of the extracted Au(III) complex was consistent with the SI and SD analyses.

Moreover, the reuse of Au(III) in $[P_{2225}][NTf_2]$ medium was investigated by continuous SX–ED processes for 10 cycles. The extraction percentage (E) of SX and the current efficiency (ε) in the ED were relatively high (E=87.0−99.4%, ε=71.9–89.3%). The efficient recovery of Au metal can be realized by the SX–ED process. The recovery yield of Au metal on each cycle was found in the range of 63.5–88.3%. The Au electrodeposits consisted mostly of metallic Au, according to the $4f_{7/2}$ XPS spectrum. This study led us to the conclusion that much of the Au metal present could be electrodeposited in metallic state from the phosphonium-based IL by the ED process. The experimental results conclude that Au metal can be continuously recovered by applying the SX–ED process using $[P_{2225}][NTf_2]$ medium.

References

[1] D. R. MacFarlane, M. Forsyth, P. C. Howlett, J. M. Pringle, J. Sun, G. Annt, W. Neil, and E.I. Izgorodina, *Acc. Chem. Res.*, **40**, 1165 (2007).

[2] M. Shamsipur, A. A. M. Beigi, M. Teymouri, S. M. Pourmortazavi, and M. Irandoust, *J. Mol. Liq.*, **157**, 43 (2010).

[3] R. Bomparola, S. Caporals, A. Lavacchi, and U. Bardi, *Surf. Coat. Technol.*, **201**, 9485 (2007).

[4] T. J. Stockmann, and Z. Ding, *J. Electroanal. Chem.*, **649**, 23 (2010).

[5] V. Stankovic´, I. Duo, Ch. Comninellis, F. Zonnevijlle, *J. Appl. Electrochem.*, **37**, 1279 (2007).

[6] Y. Song, Y. Tsuchida, M. Matsumiya, and K. Tsunashima, *Hydrometallurgy*, **181**, 164 (2018).

[7] M. Matsumiya, R. Kinoshita, Y. Tsuchida, Y. Sasaki, *J. Electrochem. Soc.*, **168**, 056501 (2021).

[8] M. Matsumiya, Y. Song, Y. Tsuchida, H. Ota, and K. Tsunashima, *Sep. Purif. Technol.*, **214**, 162 (2019).

[9] J. M. Lee, *Fluid Phase Equilib.*, **319**, 30 (2012).

[10] H. Ashkenani, and M. A. Taher, *Microchem. J.*, **103**, 185 (2012).

[11] O. Mokhodoeva, A. Nikulin, G. Myasoedova, and I. Kubrakova, *J. Anal. Chem.*, **67**, 531 (2012).

[12] B. Majidi, and F. Shemirani, *Anal. Methods*, **4**, 1072 (2012).

[13] S. Mahpishanian, and F. Shemirani, *Miner. Eng.*, **23**, 823 (2010).

[14] K. Tsunashima, and M. Sugiya, *Electrochem. Commun.*, **9(9)**, 2353 (2007).

[15] D. Nomizu, Y. Tsuchida, M. Matsumiya, and K. Tsunashima, *J. Mol. Liq.*, **318**, 114008 (2020).

[16] Y.A. Nechayev, and G.V. Zvonareva, *Geochem. Intl.*, **23**, 32 (1986).

[17] A. J. McCaffery et. al., *J. Am. Chem. Soc.*, **90(21)**, 5730 (1968).

[18] M. Castriota, T. Caruso, R. G. Agostino, E. Cazzanelli, W. A. Henderson, and S. Passerini, *J. Phys. Chem. A*, **109**, 92 (2005).

[19] Y. Umebayashi, S. Mori, K. Fujii, S. Tsuzuki, S. Seki, and S. Ishiguro, *J. Phys. Chem. B*, **114(19)**, 6513 (2010).

[20] Y. Tong, H. Yang, J. Li, and Y. Yang, *Sep. Purif. Technol.*, **120**, 367 (2013).

[21] M. Goto, and K. B. Oldham, *Anal. Chem.*, **45(12)**, 2043 (1973).

[22] P. J. Mahon, and K. B. Oldham, *J. Electroanal. Chem.*, **445**, 179 (1998).

[23] H. Matsuda, and Y. Ayabe, *Z. Elektrochem.*, **59**, 494 (1955).

[24] P. Dalrymple-alford, M. Goto, and K. B. Oldham, *J. Electroanal. Chem.*, **85**, 1 (1977).

[25] H. Vogel, *J. Physik Z.*, **22**, 645 (1921) [in German].

[26] G. S. Fulcher, *J. Amer. Ceram. Soc.*, **8(6)**, 339 (1925).

[27] G. Tammann, and W. Hesse, *Z. Anorg. Allg. Chem.*, **156(1)**, 245 (1926) [in German].

[28] S. Seki, Y. Mita, H. Tokuda, Y. Ohno, Y. Kobayashi, A. Usami, M. Watanabe, N. Terada, and H. Miyashiro, *Electrochem. Solid-State Lett.*, **10(10)**, A237 (2007).

[29] M. Matsumiya, K. Hata, K. Tsunashima, *J. Mol. Liq.*, **203**, 125 (2015).

[30] J.F. Moulder, W.F. Stickle, P.E. Sobol, and K.D. Bomben, Handbook of X-ray photoelectron spectroscopy, Perkin-Elmer Corp., Eden Prairie, MN, (1992).

Table 1 The equilibrium constant of various gold complexes formed by the hydrolysis.

Reaction	Equilibrium constant [16]
$[AuCl_4]^- + H_2O \rightleftarrows AuCl_3(H_2O) + Cl^-$	$K_1=4\times10^{-6}$
$[AuCl_3(H_2O)] \rightleftarrows [AuCl_3(OH)]^- + H^+$	$K_2=2.6\times10^{-1}$
$[AuCl_3(OH)]^- + H_2O \rightleftarrows [AuCl_2(H_2O)(OH)] + Cl^-$	$K_3=3.6\times10^{-3}$
$[AuCl_2(H_2O)(OH)] \rightleftarrows [AuCl_2(OH)_2]^- + H^+$	$K_4=2.8\times10^{-5}$
$[AuCl_2(OH)_2]^- + H_2O \rightleftarrows [AuCl(OH)_3]^- + H^+ + Cl^-$	$K_5=9.0\times10^{-9}$
$[AuCl(OH)_3]^- + H_2O \rightleftarrows [Au(OH)_4]^- + H^+ + Cl^-$	$K_6=1.0\times10^{-10}$

Table 2 Assignment of the extracted Au(III) complex in $[P_{2225}][NTf_2]$ on UV-Vis-NIR analysis.

Wavelength / nm	Molar extinction coefficient / $(mol\ dm^{-3})^{-1}\ cm^{-1}$	Assignment [17]
224.7	3.86×10^4	$^1A_{1g}\rightarrow{}^1E_u(\sigma)$
312.5	5.57×10^3	$^1A_{1g}\rightarrow{}^1A_{2u}+{}^1E_u(\pi)$

Table 3 Thermodynamic parameter of extraction for Au(III) in phosphonium-based ILs.

IL	ΔH/kJ mol^{-1}	$T\Delta S$/kJ mol^{-1}	ΔG/kJ mol^{-1}	T/K
$[P_{2225}][NTf_2]$	-9.39	-3.49	-5.90	
$[P_{2228}][NTf_2]$	-10.13	-3.68	-6.45	298.15±0.80
$[P_{22212}][NTf_2]$	-11.81	-4.38	-7.43	
$[P_{2225}][NTf_2]$	-9.39	-3.85	-5.55	
$[P_{2228}][NTf_2]$	-10.13	-4.05	-6.08	328.15±0.84
$[P_{22212}][NTf_2]$	-11.81	-4.83	-6.99	
$[P_{2225}][NTf_2]$	-9.39	-4.20	-5.19	
$[P_{2228}][NTf_2]$	-10.13	-4.42	-5.71	358.15±0.96
$[P_{22212}][NTf_2]$	-11.81	-5.27	-6.55	

Table 4 Separation factor of PGM with different types of phosphonium-based ILs.

IL	β(Au/Pt)	β(Pt/Pd)	β(Pd/Ir)	β(Ir/Ru)
$[P_{2225}][NTf_2]$	26.45	1.38	0.46	2.03
$[P_{2228}][NTf_2]$	12.05	3.78	0.24	2.54
$[P_{22212}][NTf_2]$	0.12	19.53	1.83	9.15

Table 5 VTF parameters of extracted Au(III) in phosphonium-based ILs

IL	Viscosity [14]	VTF parameters			
	η/mPa s	D_0/m^2 s^{-1}	B_D/K	$T_{0,D}$/K	R^2
[P_{2225}][NTf_2]	88	9.98×10^{-8}	-807.4	222.5	0.9651
[P_{2228}][NTf_2]	129	1.21×10^{-7}	-1119.3	201.9	0.9954
[P_{22212}][NTf_2]	180	4.33×10^{-7}	-1566.2	174.7	0.9971

Table 6 A series of recovery results of Au metal for consecutive SX and ED process at ten cycles.

No.	E /%	w_{SX} /mg	w_{res} /mg	w_{total} /mg	w_{dep} /mg	Q /C	w_{th} /mg	ε /%	R /%
1st	99.4	8.65	0.00	8.65	7.6	13.2	8.98	84.6	87.9
2nd	98.5	8.57	1.05	9.62	8.2	13.5	9.19	89.3	85.2
3rd	98.2	8.55	1.42	9.97	8.8	16.1	10.96	80.3	88.3
4th	97.3	8.47	1.17	9.63	8.3	14.6	9.93	83.5	86.1
5th	94.7	8.24	1.33	9.58	8.2	14.2	9.66	84.9	85.6
6th	92.6	8.06	1.38	9.43	7.8	15.2	10.34	75.4	82.7
7th	94.5	8.22	1.63	9.86	7.7	14.6	9.93	77.5	78.1
8th	91.5	7.96	2.16	10.12	6.9	14.1	9.59	71.9	68.2
9th	87.9	7.65	3.22	10.87	7.1	13.8	9.39	75.6	65.3
10th	87.0	7.57	3.77	11.34	7.2	13.6	9.25	77.8	63.5

E: Extraction percentage on SX, w_{SX}: Weight of extracted Au metal on SX, w_{res}:Weight of residual Au in electrolyte after ED, w_{total}: Total weight of Au metal in electrolyte ($w_{total}=w_{SX}+w_{res}$), w_{dep}: Weight of the electrodeposited Au metal, Q: Transported charge on ED, w_{th}: Theoretical weight of Au metal calculated from transported charge, ε: current efficiency ($\varepsilon=w_{dep}/w_{th}\times100$), R: recovery yield ($R=w_{dep}/w_{total}\times100$)

Captions of Figures

Fig. 1 Distribution diagram for Au(III) complexes in chloride media calculated from the equilibrium constants.

red line: [$AuCl_4^-$], brown line: [$AuCl_3(H_2O)$], pink line: [$AuCl_3(OH)^-$], green line: [$AuCl_2(OH)_2^-$], blue line: [$AuCl(OH)_3^-$] and purple line: [$Au(OH)_4^-$]

Fig. 2 UV-Vis-NIR spectrum of the Au(III) aqueous phase in 1.0 mol dm^{-3} HCl solution.

Red line:4.9 mg L^{-1} Au(III), orange line: 9.8 mg L^{-1} Au(III), green line: 24.6 mg L^{-1} Au(III), blue line: 48.2 mg L^{-1} Au(III) and purple line: 99.2 mg L^{-1} Au(III).

Fig. 3 UV-Vis-NIR spectrum of the extracted Au(III) complex in [P_{2225}][NTf_2].

The concentration of extracted Au(III) in the IL-Au complex was 2.5 mmol dm^{-3}.

Fig. 4 Raman spectra of the extracted Au(III) complex in [P_{2225}][NTf_2] system.

(a) Solvated [$Nd(NTf_2)_5^{2-}$] in [P_{2225}][NTf_2] system (red line), (b) Au(III) in [P_{2225}][NTf_2] at 318 K (orange line), (c) Au(III) in [P_{2225}][NTf_2] at 338 K (green line) and (d) Au(III) in [P_{2225}][NTf_2] at 358 K (blue line)

Fig. 5 Extraction behavior of Au(III) with different types of phosphonium-based ILs.

(a) [P_{2225}][NTf_2], (b) [P_{2228}][NTf_2] and (c) [P_{22212}][NTf_2]

The concentration of [$AuCl_4^-$] was prepared 1.0×10^2 mg dm^{-3} in 1.0 mol dm^{-3} HCl solution.

The concentration of IL was altered from 1.0×10^{-4} to 1.0×10^{-1} mol dm^{-3} for A/O=1.0.

Fig. 6 Van't Hoff plot of Au(III) with different types of phosphonium-based ILs.

(a) [P_{2225}][NTf_2], (b) [P_{2228}][NTf_2] and (c) [P_{22212}][NTf_2]

Fig. 7 Cyclic voltammogram of the extracted Au(III) complex in [P_{2225}][NTf_2] at 323 K.

Red line: 0.03 V s^{-1}, orange line: 0.05 V s^{-1}, green line: 0.07 V s^{-1} and blue line: 0.10 V s^{-1}

Fig. 8 The semi-integral analysis of the extracted Au(III) complex in $[P_{2225}][NTf_2]$ at 323 K. The scan rate is 0.10 V s^{-1}.

Fig. 9 The semi-differential analysis of the extracted Au(III) complex in $[P_{2225}][NTf_2]$ at 323 K. The scan rate is 0.10 V s^{-1}.

Fig. 10 VTF plot for the diffusion coefficients of the extracted Au(III) complex in $[P_{222X}][NTf_2]$, (X=5, 8 and 12). Red circle: Au(III) in $[P_{2225}][NTf_2]$, green circle: Au(III) in $[P_{2228}][NTf_2]$ and blue circle: $[P_{22212}][NTf_2]$, The dotted lines represent the VTF fitting: $D=D_0\exp[B/T-T_0]$.

Fig. 11 Au-4$f_{5/2}$ and 4$f_{7/2}$ spectra of 10th electrodeposits by XPS.
(a) 2nd, (b) 4th, (c) 6th, (d) 8th and (e) 10th SX-ED process

Fig. 1

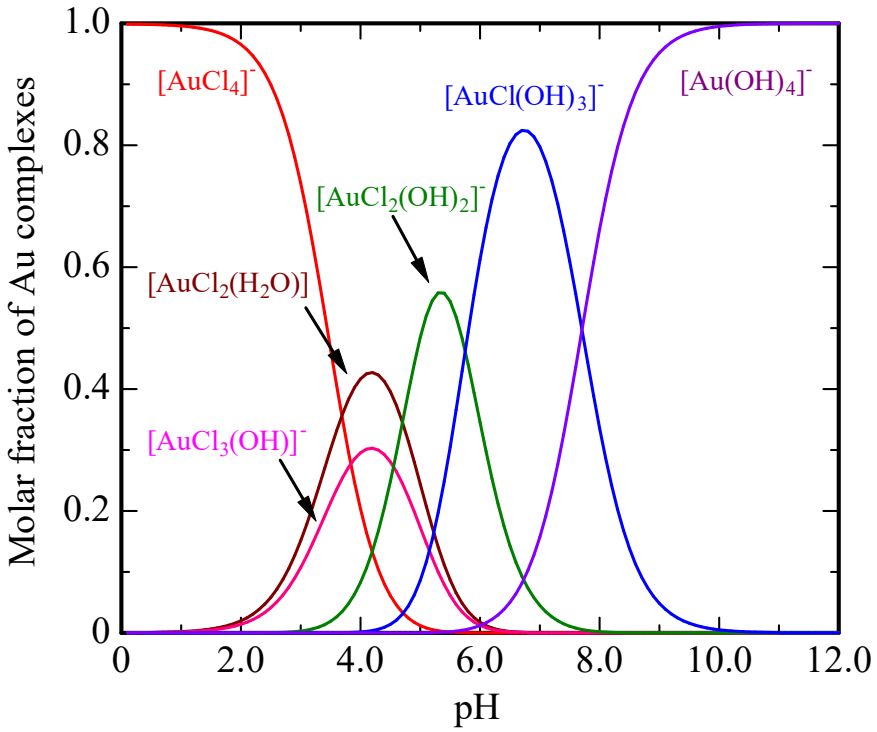
Molar fraction of Au complexes
pH
1.0
0.8
0.6
0.4
0.2
0
0
2.0
4.0
6.0
8.0
10.0
12.0
[AuCl4]-
[AuCl(OH)3]-
[Au(OH)4]-
[AuCl2(OH)2]-
[AuCl2(H2O)]
[AuCl3(OH)]-

Fig.2

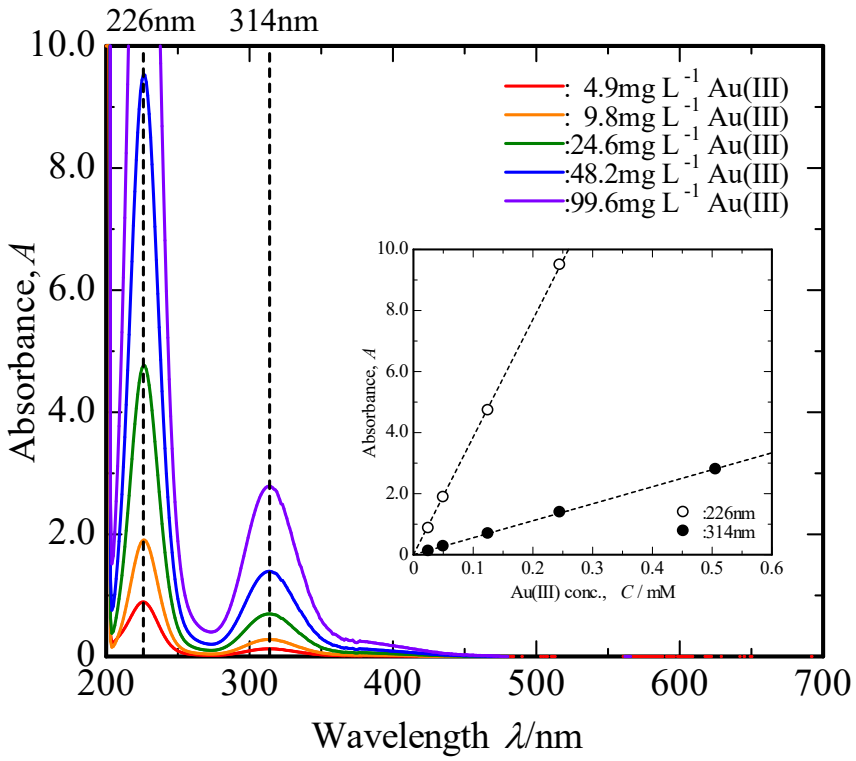
226nm
314nm
: 4.9mg L -1 Au(III)
: 9.8mg L -1 Au(III)
:24.6mg L -1 Au(III)
:48.2mg L -1 Au(III)
:99.6mg L -1 Au(III)
Absorbance, A
Wavelength λ/nm
Absorbance, A
Au(III) conc., C / mM
:226nm
:314nm

Fig. 3

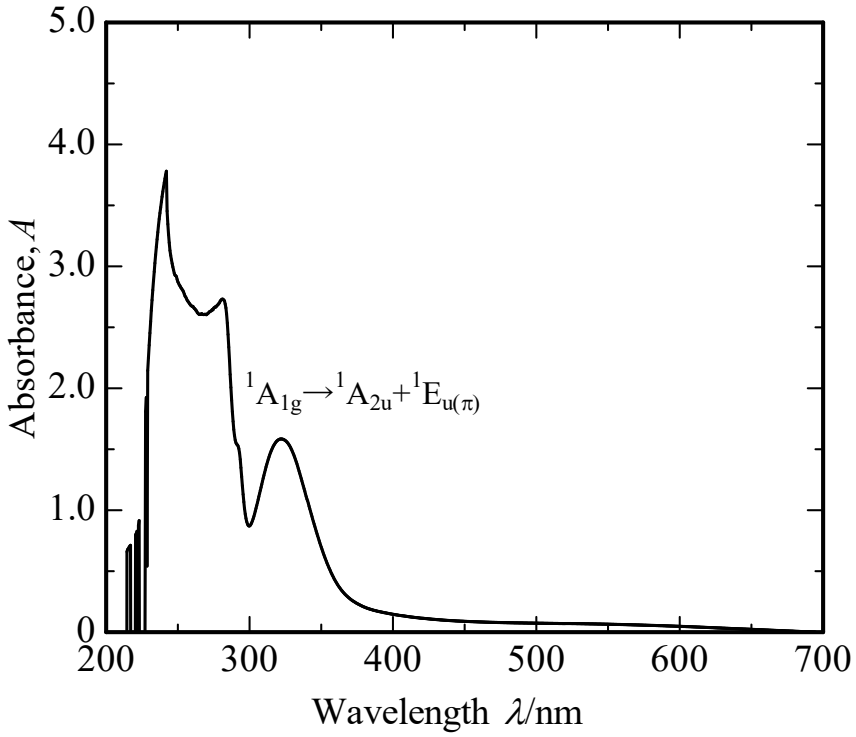
5.0
4.0
3.0
2.0
1.0
0
Absorbance, A
200
300
400
500
600
700
Wavelength λ/nm
$^1A_{1g} \rightarrow {}^1A_{2u} + {}^1E_{u(\pi)}$

Fig. 4

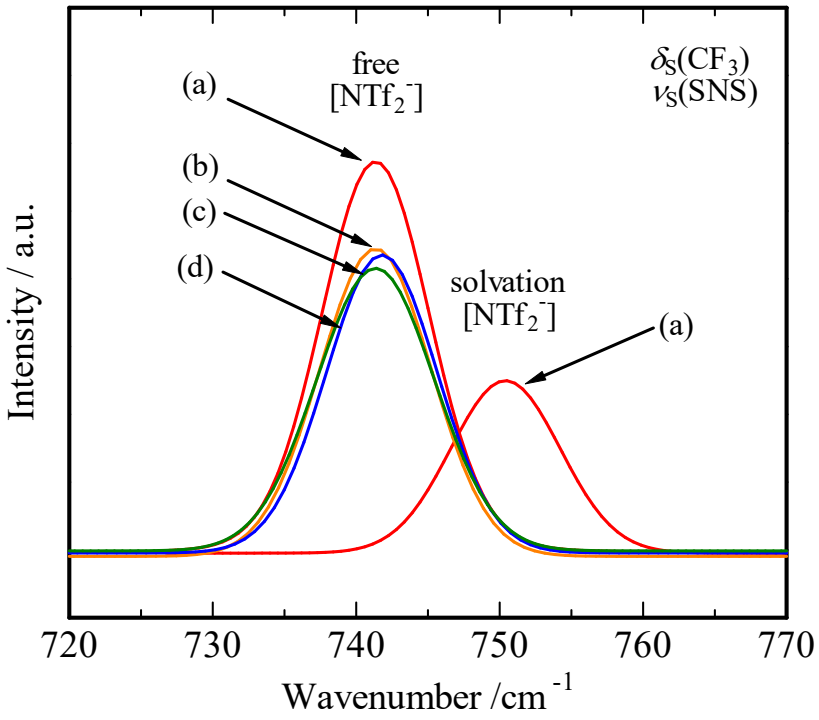
free
[NTf2-]
δS(CF3)
νS(SNS)
(a)
(b)
(c)
(d)
solvation
[NTf2-]
(a)
Intensity / a.u.
720
730
740
750
760
770
Wavenumber /cm-1

Fig. 5

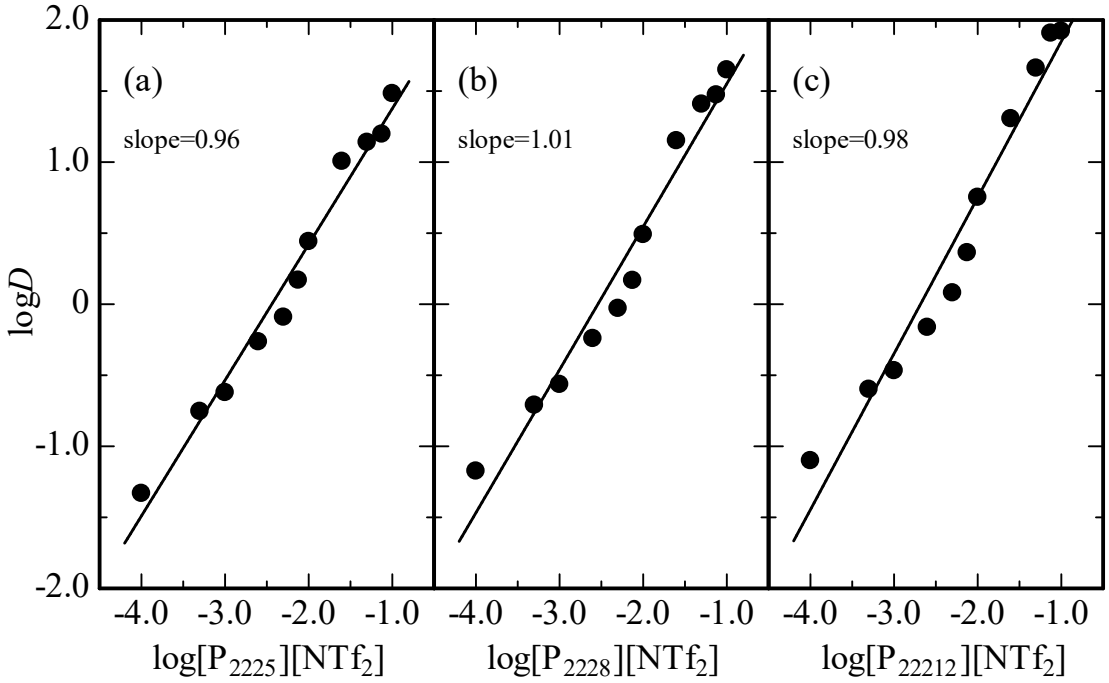
2.0
1.0
0
-1.0
-2.0
logD
(a)
slope=0.96
(b)
slope=1.01
(c)
slope=0.98
-4.0 -3.0 -2.0 -1.0
log[P2225][NTf2]
log[P2228][NTf2]
log[P22212][NTf2]

Fig. 6

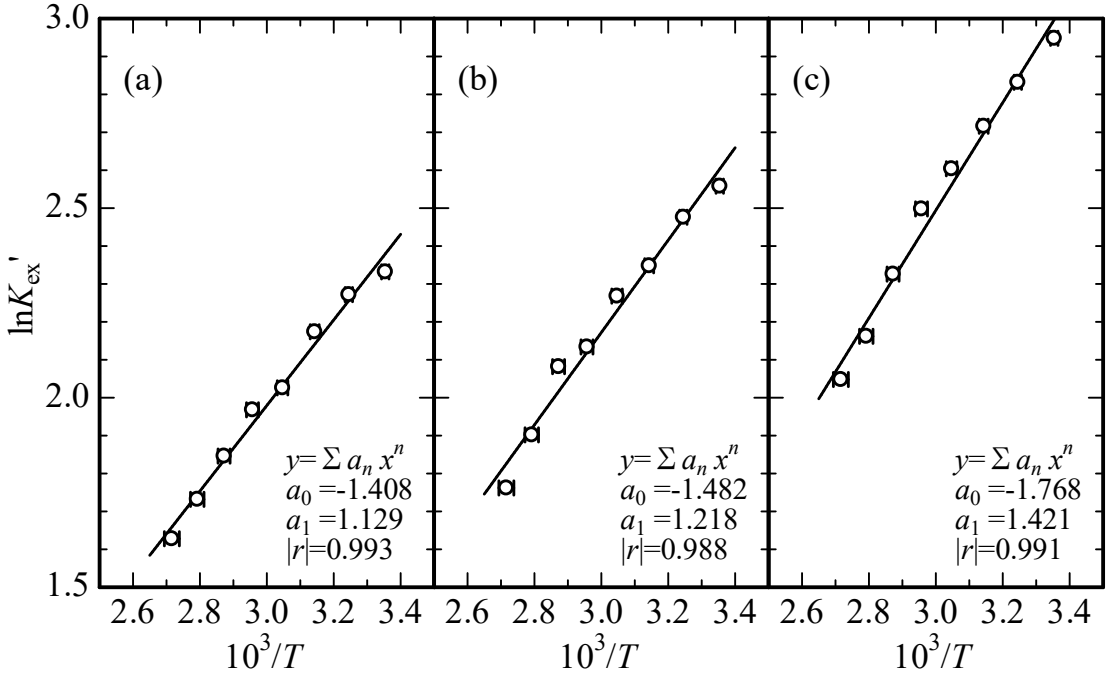
(a)
(b)
(c)
$y=\Sigma\, a_n\, x^n$
a_0 =-1.408
a_1 =1.129
|r|=0.993
$y=\Sigma\, a_n\, x^n$
a_0 =-1.482
a_1 =1.218
|r|=0.988
$y=\Sigma\, a_n\, x^n$
a_0 =-1.768
a_1 =1.421
|r|=0.991
lnK_{ex}'
3.0
2.5
2.0
1.5
2.6 2.8 3.0 3.2 3.4
$10^3/T$

Fig. 7

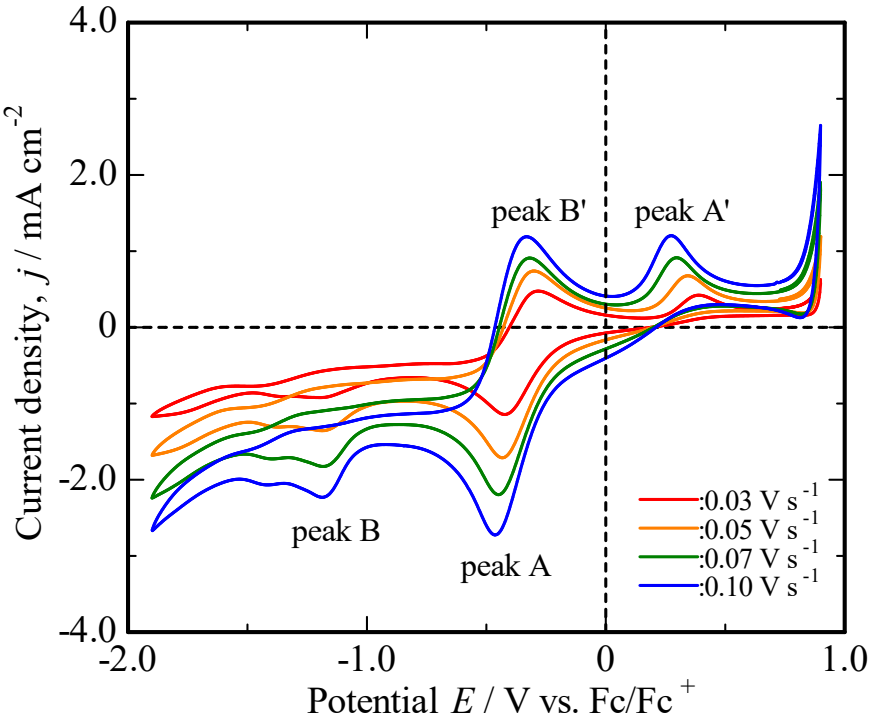
4.0
2.0
0
-2.0
-4.0
-2.0
-1.0
0
1.0
Current density, j / mA cm-2
Potential E / V vs. Fc/Fc+
peak B'
peak A'
peak B
peak A
:0.03 V s-1
:0.05 V s-1
:0.07 V s-1
:0.10 V s-1

Fig. 8

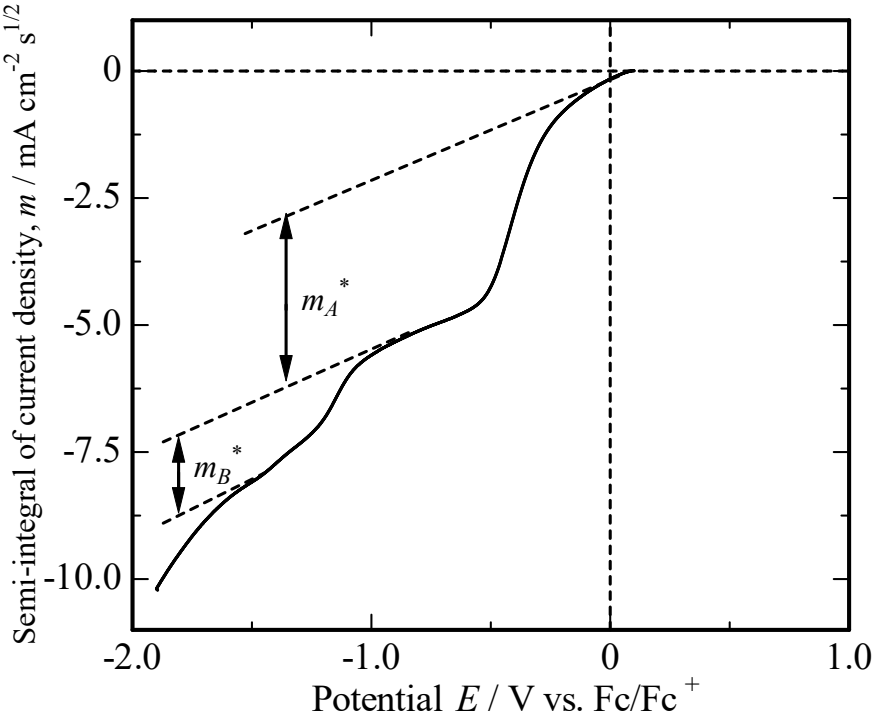
Semi-integral of current density, m / mA cm-2 s1/2
0
-2.5
-5.0
-7.5
-10.0
-2.0
-1.0
0
1.0
Potential E / V vs. Fc/Fc+
mA*
mB*

Fig. 9

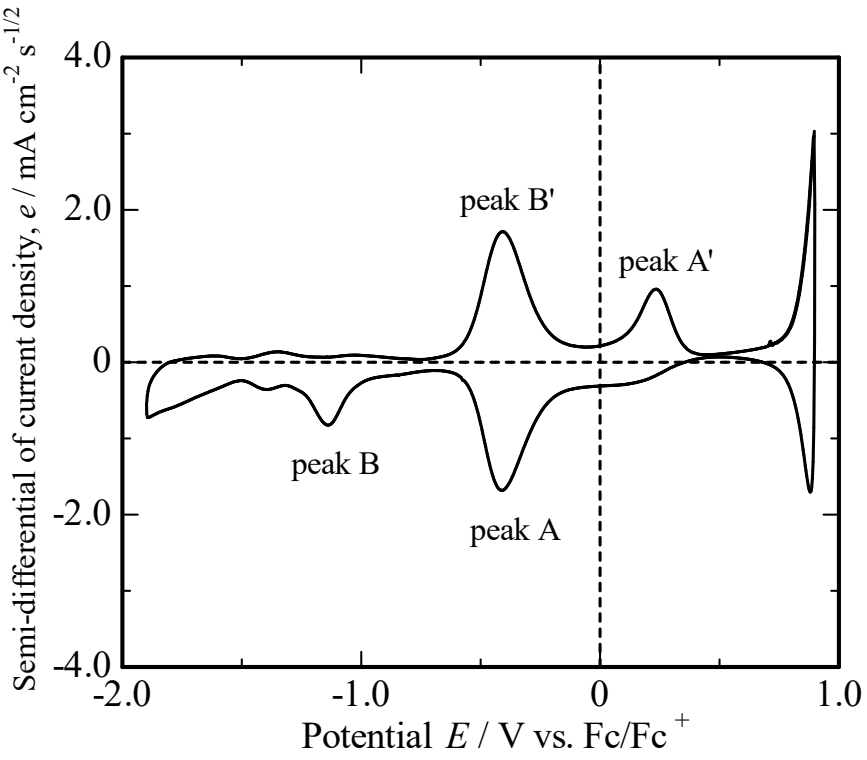
Semi-differential of current density, e / mA cm-2 s-1/2
4.0
2.0
0
-2.0
-4.0
-2.0
-1.0
0
1.0
Potential E / V vs. Fc/Fc+
peak B'
peak A'
peak B
peak A

Fig. 10

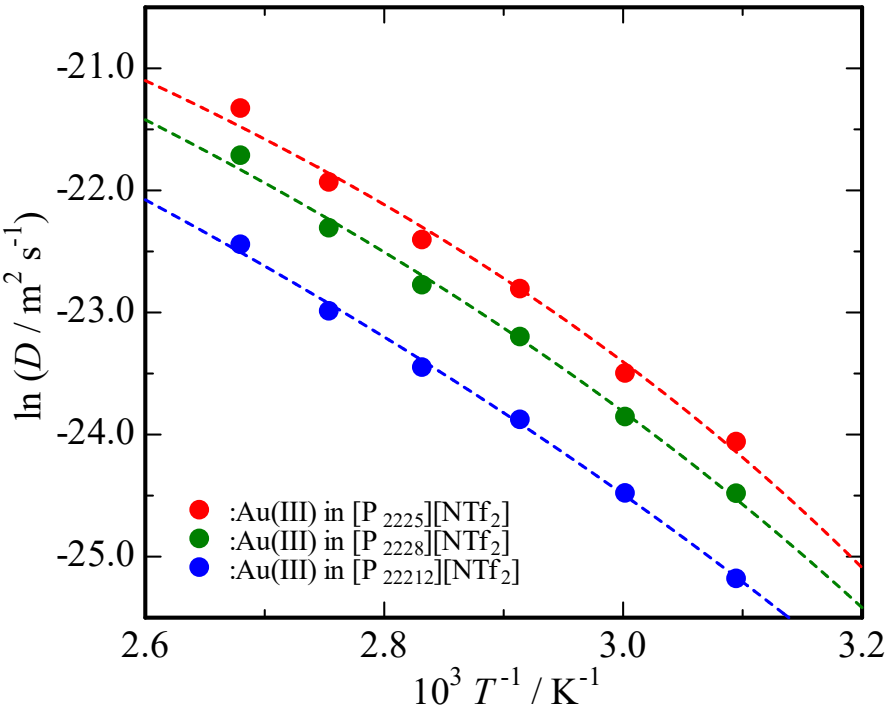
-21.0
-22.0
-23.0
-24.0
-25.0
ln (D / m2 s-1)
2.6
2.8
3.0
3.2
103 T-1 / K-1
:Au(III) in [P 2225][NTf2]
:Au(III) in [P 2228][NTf2]
:Au(III) in [P 22212][NTf2]

Fig. 11